Available online at www.sciencedirect.com

ScienceDirect

Advances in Space Research 56 (2015) 1578–1589

Advances in Space Research
(a COSPAR publication)

www.elsevier.com/locate/asr

A physical algorithm to measure sea ice concentration from passive microwave remote sensing data

V.V. Tikhonov [a,*], I.A. Repina [a,b,c], M.D. Raev [a], E.A. Sharkov [a], V.V. Ivanov [c,d], D.A. Boyarskii [a], T.A. Alexeeva [d], N.Yu. Komarova [a]

[a] Department of Earth Research from Space, Space Research Institute, Russian Academy of Sciences, Moscow, Russia
[b] Air-Sea Interaction Lab., A.M. Obukhov Institute of Atmospheric Physics, Russian Academy of Sciences, Moscow, Russia
[c] Hydrometeorological Centre of Russia, Moscow, Russia
[d] Arctic and Antarctic Research Institute, Saint-Petersburg, Russia

Received 8 February 2015; received in revised form 7 July 2015; accepted 8 July 2015
Available online 14 July 2015

Abstract

A conceptually new algorithm of sea ice concentration retrieval in polar regions from satellite microwave radiometry data is discussed. The algorithm design favorably contrasts with that of known modern algorithms. Its design is based on a physical emission model of the "sea surface – sea ice – snow cover – atmosphere" system. No tie-points are used in the algorithm. All the calculation expressions are derived from theoretical modeling. The design of the algorithm minimizes the impact of atmospheric variability on sea ice concentration retrieval. Beside estimating sea ice concentration, the algorithm makes it possible to indicate ice areas with melting snow and melt ponds. The algorithm is simple to use, no complicated or time consuming calculations are involved.

Keywords: Microwave radiometry; Sea ice; Melting snow

1. Introduction

Vast areas occupied by sea ice and its seasonal variability are in the focus of serious scientific studies. They have gained importance in recent decades as climate change has become a major global social and political issue. Since the polar regions are hard to reach and meteorological stations there are rather scarce, remote sensing techniques to investigate sea ice are in high demand. Active and passive instruments operating in microwave range on board Earth satellites make measurements regardless of the time of the day or cloudiness. Passive remote sensing instruments are the most adequate ones in terms of temporal (sensing duration and recurrence) and spatial (swath width and overlap) coverage (Carsey, 1992; Comiso, 2009; Massom and Lubin, 2006; Rees, 2006; Teleti and Luis, 2013).

Nevertheless, for various reasons, the techniques employed today to retrieve ice cover characteristics from passive microwave remote sensing data give significant errors (Agnew and Howell, 2003; Andersen et al., 2007; Carsey, 1992; Cavalieri et al., 1995; Comiso and Kwok, 1996; Fetterer and Untersteiner, 1998; Ivanova et al., 2014, 2015; Meier, 2005).

Analysis of ice concentration retrieval by various algorithms, intercomparison of the results, comparison of the results with optical and radar observations, as well as visual observations from ships show that errors of the algorithms currently in use reach 10% (Andersen et al., 2007;

* Corresponding author at: Department of Earth Research from Space, Space Research Institute, Russian Academy of Sciences, Profsojuznaya, 84/32, Moscow 117997, Russia.
E-mail address: vtikhonov@asp.iki.rssi.ru (V.V. Tikhonov).

http://dx.doi.org/10.1016/j.asr.2015.07.009
0273-1177/

Meier et al., 2001; Meier, 2005; Spreen et al., 2008). In periods of summer melt and autumn freeze-up the errors rise dramatically, sometimes up to 50% (Agnew and Howell, 2003; Andersen et al., 2007; Ivanova et al., 2014; Knuth and Ackley, 2006; Meier et al., 2001; Spreen et al., 2008). The majority of authors note the following reasons for the errors in ice concentration retrieval by the algorithms from satellite microwave radiometry data:

– inability to separate emission from more than two ice types (see, for example, Teleti and Luis, 2013);
– seasonal variability of sea ice and snow emissivity (Agnew and Howell, 2003; Ivanova et al., 2015; Knuth and Ackley, 2006; Spreen et al., 2008);
– non-seasonal regional variability of snow and ice surface emissivity (Agnew and Howell, 2003; Ivanova et al., 2015; Knuth and Ackley, 2006; Spreen et al., 2008);
– surface effects, such as surface roughness, snow cover, melting snow, and melt ponds (Andersen et al., 2007; Hewison et al., 2002; Knuth and Ackley, 2006);
– weather effects, such as precipitation (rain, snow, snowstorm, etc.) (Andersen et al., 2006, 2007; Cho and Nishiura, 2010).

Dividing ice into types (multiyear, first-year, etc.) from satellite microwave radiometry data is an important, but practically unattainable goal. The solution is attempted based on the differences in frequency dependencies of emissivity or brightness temperature of different ice types. However, the dependencies were obtained by in-situ measurements (Spreen et al., 2008) for level and clean ice surface. The radiometer spots in those measurements were several meters in size (see, for example, Comiso et al., 1989). For satellite microwave radiometers, pixel size is over 10 km. Emissivity of such extended area is determined not only by the ice type, but also the surface roughness and snow cover. Theoretical estimates demonstrate that dry snow penetration depth at frequencies over 19 GHz is less than 40 cm (Tikhonov et al., 2013, 2014). Therefore, a layer of snow on ice will change considerably the brightness temperature difference between multiyear and first-year ice. Brightness temperature values retrieved from satellite data are significantly affected by surface roughness. These statements were proved by many experimental and theoretical studies (Agnew and Howell, 2003; Cavalieri and Comiso, 2000; Comiso et al., 1989; Hewison et al., 2002; Matzler, 2000; Powell et al., 2006). It is unclear how to select ice type if both multiyear and first-year ice types are present within a pixel area. Notice, that many currently used algorithms produce concentration of ice not specifying its type or age (NASA Team 2, Bootstrap, ARTIST Sea Ice). However, in some cases existing algorithms (e.g. NASA Team, NORSEXS, ECICE) allow reasonable distinguishing of various types of ice (Han and Lee, 2006; Shokr et al., 2008; Svendsen et al., 1983; Voss et al., 2003). Probably, this happens when the ice is flat and there is no snow cover.

Fixed values of emissivity, brightness or physical temperature of ice or open water surface, called tie-points, are widely used in the algorithms. This also leads to considerable errors in calculated ice concentration (Agnew and Howell, 2003; Andersen, 1998). The emissivity of ice, even if it is one-type ice, cannot always remain constant. It depends on surface temperature and climate conditions during formation. Ice emissivity is affected by its snow cover, whose thickness, structure and wetness vary depending on the season and region of formation. Sea ice emissivity is also conditioned by surface roughness that has regional and seasonal characteristics as well.

Elimination of errors in ice concentration retrieval essentially addresses two problems: better account for atmospheric properties and higher accuracy of tie-points determination (Andersen et al., 2006; Cavalieri and Comiso, 2000; Cho and Nishiura, 2010; Comiso, 1995; Ivanova et al., 2014; Kaleschke et al., 2001; Kern, 2004; Lovas et al., 1994; Meier et al., 2001; Pedersen, 1994; Spreen et al., 2008). Attempts in the first direction represent algorithms SEA LION (Kern, 2004), CalVal (Meier et al., 2001), NASA Team (Cho and Nishiura, 2010), NASA Team 2 (Cavalieri and Comiso, 2000), and ASI (Spreen et al., 2008) using various atmospheric models and methods to reduce atmospheric effects. The second problem is addressed by all algorithms since tie-points determination is the principal stage in ice concentration retrieval from microwave satellite data. In particular, it was suggested to introduce dynamical tie-points, that is to determine tie-points individually for different regions and seasons (Agnew and Howell, 2003; Andersen, 1998; Ivanova et al., 2015). Employing dynamical tie-points raises the accuracy of the algorithms (Agnew and Howell, 2003; Andersen, 1998; Ivanova et al., 2015). However, such approach also makes them more difficult to use as tie-point values vary depending on region and season. Consequently, the tie-points should be monitored continuously on regional and seasonal scales. The problem cannot be solved once and for all in conditions of gradual climate transformation. Ice and snow cover climatic formation conditions are changing, which affects surface emission properties as well. The examples are algorithms ASI and Bootstrap, whose tie-point values were modified as time passed (Comiso, 1995; Kaleschke et al., 2001).

In the paper, we discuss a possibility to develop a principally new class of algorithms to retrieve sea ice concentration from microwave satellite radiometry data. Such an algorithm is based solely on a model of emissivity of the "sea surface – sea ice – snow cover – atmosphere" system. It does not use tie-points. Input parameters are real physical and structural properties of sea ice and snow cover (temperature, density, wetness, etc.) of the Arctic and Antarctic, as well as climate characteristics (air temperature and humidity, atmospheric pressure, etc.) of the regions. The schematic of the algorithm is given in Section 2. Section 3 describes the use of satellite and ship observation data for validation of the algorithm. A comparison of the proposed algorithm calculations of sea ice concentration in the Arctic and Antarctic and ship visual observation data is presented in Section 4.

2. An integrated algorithm for sea ice concentration determination

Experimental data on emissivity or brightness temperature of sea ice and open water provide the foundation of modern algorithms (Grenfell and Comiso, 1986; Swift et al., 1992). The experiments were carried out in the Fram Strait, Greenland, Bering, Beaufort and Chukchi Seas in the Arctic, and Weddell Sea in the Antarctic (Onstott et al., 1987; Tucker et al., 1991; Grenfell, 1986, 1992; Flückiger et al., 1994; Drinkwater et al., 1991; Comiso et al., 1989). Airborne radiometric observations and satellite data are also used for this task (Cavalieri et al., 1986).

The algorithm introduced in this paper fundamentally differs from all others. The principal feature of this algorithm is that it is based on a theoretical model of emissivity of the system "sea surface – sea ice – snow cover – atmosphere", not just experimental data (Tikhonov et al., 2014). The model includes: emission model of a layered medium (Sharkov, 2003), a model of dielectric properties of ice and snow (Boyarskii et al., 1994; Tikhonov et al., 2014), a standard atmosphere model (Tikhonov et al., 2014), a model of surface roughness in the microwave range (Choudhury et al., 1979). Antenna pattern and radiometer bandwidth were taken into account in the model calculations.

The algorithm development required finding the model parameters determined by ice concentration but resistant to changes in physical characteristics of the surface and weakly dependent on atmospheric changes. The analysis of the model calculations of ice cover brightness temperature in the Arctic and their comparison with the SSM/I (Special Sensor Microwave/Imager) and SSMIS (Special Sensor Microwave Imager Sounder) data (Tikhonov et al., 2013, 2014) have shown that the sought parameters may be tangents of the angles between the lines drawn through the brightness temperature values at two different frequencies of the same polarization and the frequency axis:

$$t^v_{85-19} = \frac{T^v_{85} - T^v_{19}}{85.5 - 19.35}, \quad t^v_{85-37} = \frac{T^v_{85} - T^v_{37}}{85.5 - 37}, \quad t^v_{37-19} = \frac{T^v_{37} - T^v_{19}}{37 - 19.35},$$
$$t^h_{85-19} = \frac{T^h_{85} - T^h_{19}}{85.5 - 19.35}, \quad t^h_{85-37} = \frac{T^h_{85} - T^h_{37}}{85.5 - 37}, \quad t^h_{37-19} = \frac{T^h_{37} - T^h_{19}}{37 - 19.35}, \tag{1}$$

where T^p_f is the brightness temperature for frequency f and polarization p. Calculations for all tangents were performed by Eq. (1) at different physical and structural characteristics of the surface (ice concentration and type, temperature and thickness of snow cover, volumetric wetnesses of snow and ice, surface roughness, etc.). The range of these characteristics has been selected in accordance with the climatic and glaciological data of the polar regions (Gray and Male, 1981; Przybylak, 2003; Serreze and Barry, 2005; Turner et al., 2009; Cuffey and Paterson, 2010). Air temperature was taken in the range from −50 to +10 °C, the temperature of ice or snow surface from −50 to 0 °C, water temperature from −1.8 to +5 °C, ice concentration from 0 to 100%, the thickness of snow cover from 0 to 60 cm, volumetric wetness of ice from 0 to the maximum saturation, volumetric wetness of snow from 0 to 30%, air and salt inclusion in ice from 5 to 40% of unit volume, surface roughness from a smooth surface to a roughness comparable with the size of emission wavelength. The results of calculations are presented in Fig. 1. The shaded areas denote the tangent values at different structural and physical characteristics of the surface.

Analysis of the dependencies in Fig. 1 reveals two tangent values apparently stable to changes in surface characteristics. They are the tangent at frequencies 85.5 GHz and 19.35 GHz on vertical polarization (85–19 v), and the tangent at frequencies 85.5 GHz and 37 GHz on horizontal polarization (85–37 h) (Fig. 1(a) and (e)). The tangent at frequencies 85.5 GHz and 37 GHz on vertical polarization (Fig. 1(b)) is also rather insensitive to a change in surface characteristics. However, it is weakly dependent on changes in ice concentration.

The value ranges of the two selected tangents were averaged by linear functions that depend only on the ice cover concentration (dashed lines in Fig. 1(a) and (e)):

$$f^h_{85-37}(I) = -0.085 \times I + 0.908, \tag{2}$$

$$f^v_{85-19}(I) = -0.086 \times I + 0.55, \tag{3}$$

where I is ice concentration expressed in 10ths.

Expressions Eqs. (2) and (3) allow us to reconstruct ice concentration from satellite radiometer (e.g., SSM/I) data combinations of bands 85 and 19 GHz on vertical polarization and bands 85 and 37 GHz on horizontal polarization. The use of two parameters (tangents) and their linear approximations is explained by the fact that they depend in a different manner on different physical and structural characteristics of the surface. This is linked with different sensitivities of frequencies and polarizations to variation of these characteristics. For instance, the emissivity at 85.5 GHz is largely affected by scattering in the surface layer of snow or ice (Andersen et al., 2007). The low-frequency bands (19.35 and 37 GHz) are more sensitive to volumetric scattering in snow and ice covers (Andersen et al., 2007; Boyarskii et al., 1994; Boyarskii and Tikhonov, 2000). This is explained by a greater penetration depth at these frequencies (Tikhonov et al., 2014) and dimension similarity between inhomogeneities and emission wavelength (Boyarskii et al., 1994; Boyarskii and Tikhonov, 2000). Horizontal polarization bands are more sensitive to stratification of snow cover and sea ice (Andersen et al., 2007). Snow wetness variations have greater effect at 37 GHz (Boyarskii and Tikhonov, 2000).

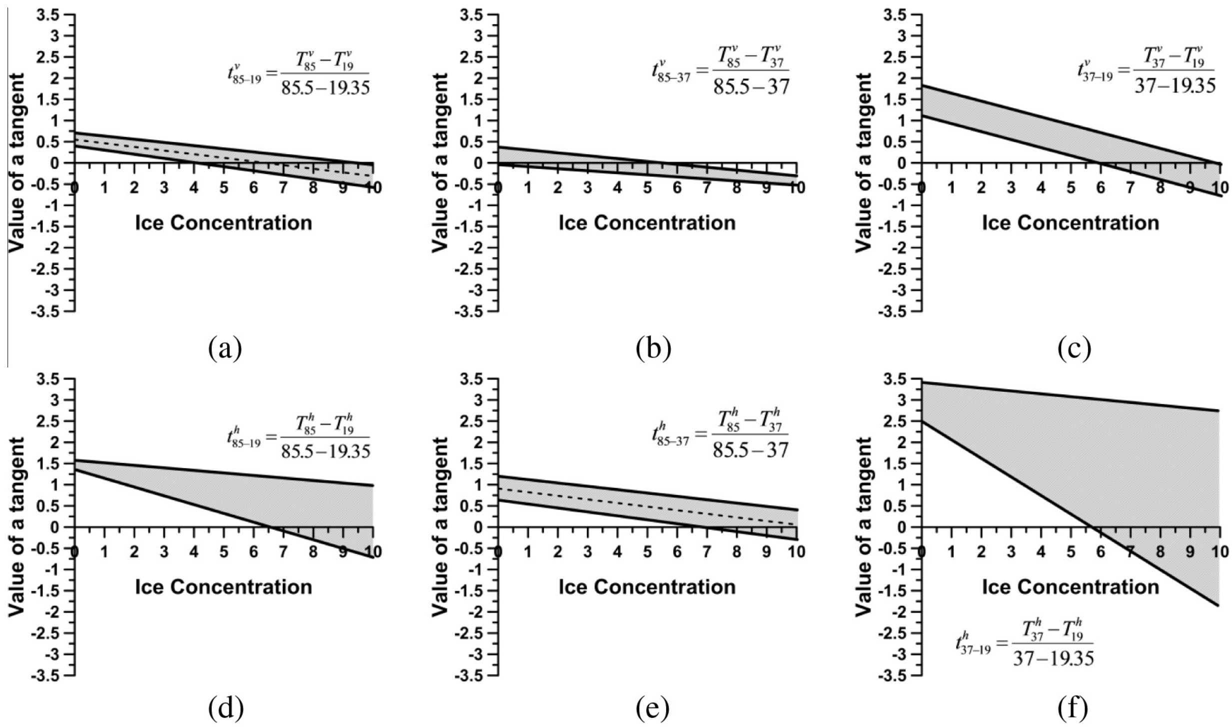

Fig. 1. Dependencies of the tangent values (shaded areas) on ice concentration: (a) 85–19 v, (b) 85–37 v, (c) 37–19 v, (d) 85–18 h, (e) 85–37 h, (f) 37–19 h.

Thus, the two parameters (Eqs. (2) and (3)) may be considered complementary to each other in determining ice concentration.

Based on Eqs. (2) and (3) dependencies, an algorithm, called Variation Arctic/Antarctic Sea Ice Algorithm (VASIA), for ice concentration determination from satellite microwave radiometer data in the polar regions was developed.

A comparison of ice concentrations retrieved by VASIA and NASA Team 2 shows that the former gives underestimated values for the summer months. This is explained by the presence of melting snow on the ice surface. Such ice areas are referred to as ice having significant surface effects by NASA Team 2 (Cavalieri and Comiso, 2000; Markus and Cavalieri, 2009).

Normally, snow cover can contain approximately 9–30% of liquid water in a unit volume depending on the density and structure of snow (Kotlyakov, 2000; Kuz'min, 1957). The excess water drains down. If the snow is on top of ice and no drainage is possible, a snow–water mixture (SWM) occurs. The final form of snow–water mixture evolution is melt pond. (We assume SWM to be a snow cover with a wetness from 30% to melt pond.) Melt ponds are an important element of the Arctic climate system. They can occupy up to 50% of the total ice cover (Istomina et al., 2014; Polashenski et al., 2012; Rösel and Kaleschke, 2012; Rösel et al., 2012; Tschudi et al., 2008) and play an important role in ocean and atmosphere interaction. Because of low albedo they absorb multiple times greater short-wave radiation than the rest of the snow and ice cover (Grenfell and Perovich, 1984; Tschudi et al., 2008). The depth of melt ponds can vary from a few centimeters to 1.5 meters (Morassutti and Ledrew, 1996; Perovich et al., 2003). Their horizontal size can reach hundreds of square meters (Polashenski et al., 2012; Tucker et al., 1999). In the Antarctic, melt ponds are less frequent due to cooler and drier conditions in summer, as well as too thick a snow cover to be able to melt down during summer months (Thomas and Dieckmann, 2003).

Since VASIA algorithm is based on an electrodynamic model of emissivity of the "sea surface – sea ice – snow cover – atmosphere" system, it reflects the real structure of the surface. The appearance of liquid water in snow leads to considerable increase of the real and imaginary parts of wet snow dielectric constant in the microwave range. These dependencies are identical in shape to those of the real and imaginary parts of water (Tikhonov et al., 2014). Therefore, the emissivity of wet snow is determined primarily by the volumetric content of liquid water in the snow (Boyarskii and Tikhonov, 2000; Matzler and Huppi, 1989). The penetration depth of wet snow at frequencies over 19 GHz is less than 1 cm (Matzler, 2006; Tikhonov et al., 2014). The content of liquid water in SWM is larger than in wet snow. Hence, by radiometric data, even a very thin SWM layer closely resembles a low ice concentration area. This is the reason for VASIA strong underestimation of ice concentration in summer.

To overcome this problem, a model of effective dielectric constant of SWM has been developed. From the electrodynamics point of view, SWM is a mixture of three media: water, ice and air. Because SWM volumetric water content is large (>30%), its dielectric properties are mainly determined by radiation absorption by liquid water (Tikhonov et al., 2014). The effective dielectric constant can be defined using electrostatic dielectric mixture models. We chose the Polder–Van Santen model (Polder and van Santen, 1946) known to provide a satisfactory description of snow cover dielectric properties (Hallikainen et al., 1986; Sihvola and Kong, 1988; Boyarskii et al., 1994). It was used in the emission model of the "sea surface – sea ice – snow cover – atmosphere" system (Tikhonov et al., 2014) to calculate brightness temperature of sea ice with SWM. Calculations were performed for SWM with volumetric water content from 30% to 100% (melt pond). The calculation results for two previously selected tangents (Fig. 1(a) and (e)) are presented in Fig. 2.

The shaded triangles in the figure denote the ranges of tangent values for SWM on top of ice. The upper sides correspond to melt pond (100% water), while the lower sides to 30% content of water in SWM. The SWM tangent value ranges were approximated by linear functions depending solely on ice concentration (dash-dot lines in Fig. 2):

$$\varphi^{h}_{85\text{–}37}(I) = -0.039 \times I + 1.19, \quad (4)$$

$$\varphi^{v}_{85\text{–}19}(I) = -0.04 \times I + 0.7, \quad (5)$$

where I is ice concentration expressed in 10ths.

Hence, in case there is SWM on top of ice surface, ice concentration should be calculated by Eqs. (4) and (5) rather than Eqs. (2) and (3). The tangent for 37 and 19.35 GHz on vertical polarization (37–19 v) was selected as a criterion for using the approximation of Eqs. (2) and (3) or Eqs. (4) and (5). The dependence of tangent 37–19 v on ice concentration is shown in Fig. 3. The selection of the criterion is justified by the strong dependence of tangent 37–19 v on moisture content of surface layer: the shaded triangle in Fig. 3 is much larger than the shaded triangles in Fig. 2.

In the general case, the tangent 37–19 v values for different ice concentrations (Fig. 3) will be either in region 1 (ice covered by snow and clean ice) or inside the shaded triangle – region 2 (ice with SWM). In real physical and structural conditions of the surface layer, the tangent values may not exist outside these regions. The top line of region 2 corresponds to open water surface. The bottom line of region 1 defines another limit of possible values of physical and structural parameters of the surface layer (temperature, wetness, density, porosity, etc.). At a certain ice concentration, values of the three tangents (85–19 v, 85–37 h and 37–19 v) must fall within the permitted region and correspond to one ice concentration value. If the two main tangents (85–19 v, 85–37 h) point out ice concentration equal to 10%, then tangent 37–19 v must give the same ice concentration and drop within the allowed region (1) and (2). If a tangent 37–19 v value appears to be in the forbidden region (left ellipse in Fig. 3), it means that ice concentration is defined incorrectly. In this case, the allowed values of tangent 37–19 v are in the region of high concentration (e.g., the right ellipse in Fig. 3), which corresponds to presence of SWM on the surface of ice. The lower boundary of region 1 was chosen as the criterion of SWM presence on ice. If, at a certain concentration, a tangent 37–19 v value falls below this boundary, then there is SWM on ice and ice concentration should be calculated by Eqs. (4) and (5).

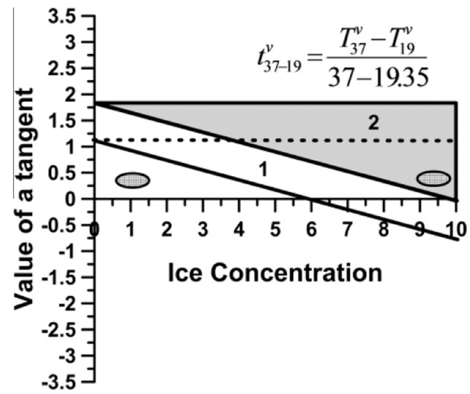

Fig. 3. Dependence of tangent 37–19 v on ice concentration for ice with SWM on the surface (shaded triangle).

The lower boundary of region 1 (Fig. 3) was approximated by a linear function that depends only on ice concentration I:

$$\delta^{v}_{37\text{–}19}(I) = -0.187 \times I + 1.1. \quad (6)$$

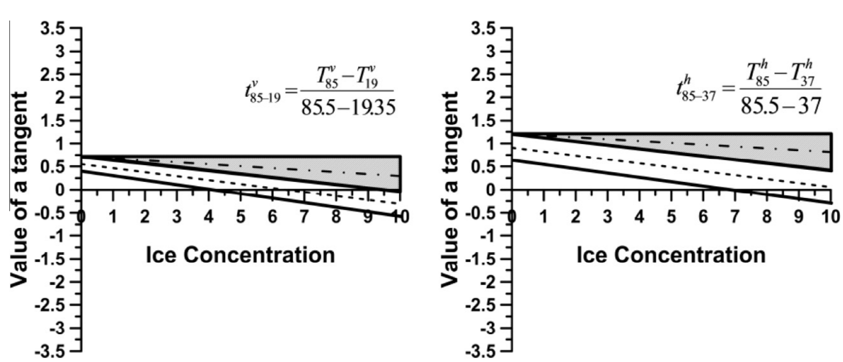

Fig. 2. Dependencies of tangents (a) 85–19 v and (b) 85–37 h on ice concentration for ice with SWM on the surface (shaded triangles).

The new algorithm, called VASIA2, was developed on the basis of these relationships. The schematic of the algorithm is as follows.

1. Three tangents (satellite tangents), namely, 85–37 h, 85–19 v and 37–19 v are calculated from microwave satellite data:

$$t^h_{85\text{–}37} = \frac{T^h_{85} - T^h_{37}}{85.5 - 37}, \quad t^v_{85\text{–}19} = \frac{T^v_{85} - T^v_{19}}{85.5 - 19.35}, \quad t^v_{37\text{–}19} = \frac{T^v_{37} - T^v_{19}}{37 - 19.35}.$$

2. Criterion function F_1 is constructed as the sum of squared coefficients of variation between the theoretical tangent values given by Eqs. (2) and (3) and the values of satellite tangents 85–37 h and 85–19 v:

$$F_1 = \frac{1}{2}\left[\frac{\left(f^h_{85\text{–}37}(I) - t^h_{85\text{–}37}\right)^2}{\left(t^h_{85\text{–}37}\right)^2} + \frac{\left(f^v_{85\text{–}19}(I) - t^v_{85\text{–}19}\right)^2}{\left(t^v_{85\text{–}19}\right)^2}\right].$$

3. Criterion function F_1 is calculated for ice concentration from 0 to 10 with a step equal to 0.1. (Note: ice concentration is expressed in 10ths).
4. The minimum value of criterion function F_1 determines the ice concentration I_1. I_1 is sea ice concentration without error correction related to SWM on ice. This is ice concentration given by VASIA algorithm. Steps 1–4 are therefore the same as in VASIA.
5. At the given I_1, for each pixel the value calculated by Eq. (6) is compared to the value of satellite tangent 37–19 v:

$$\delta^v_{37\text{–}19}(I_1) \quad ? \quad t^v_{37\text{–}19}.$$

6. If: $\delta^v_{37\text{–}19}(I_1) < t^v_{37\text{–}19}$, then the ice concentration is taken equal to the one determined at Step 4:

$$I_2 = I_1.$$

7. If: $\delta^v_{37\text{–}19}(I_1) \geqslant t^v_{37\text{–}19}$, then the criterion function F_2 is constructed as the sum of squared coefficients of variation between the theoretical tangent values given by Eqs. (4) and (5) and the values of satellite tangents 85–37 h and 85–19 v:

$$F_2 = \frac{1}{2}\left[\frac{\left(\varphi^h_{85\text{–}37}(I) - t^h_{85\text{–}37}\right)^2}{\left(t^h_{85\text{–}37}\right)^2} + \frac{\left(\varphi^v_{85\text{–}19}(I) - t^v_{85\text{–}19}\right)^2}{\left(t^v_{85\text{–}19}\right)^2}\right]$$

8. For the interval of ice concentrations from 0 to 10, the minimum value of criterion function F_2 is found.
9. The minimum value of criterion function F_2 determines the final ice concentration I_2.

Ice concentration I_2 corresponds to the real ice concentration in the given pixel. The difference between concentrations obtained at Steps 9 and 4 (I_2–I_1 or VASIA2–VASIA) shows the specific area occupied by SWM on the surface of ice.

Linear functions expressed by Eqs. (2), (3) and Eqs. (4), (5) are approximations of theoretical tangents calculated for SSM/I radiometer bands (19.35, 37 and 85.5 GHz). However, further calculations demonstrated their validity also for SSMIS (bands 19.35, 37 and 91,655 GHz) and AMSR2 (bands 18.7, 36.5 and 89 GHz) radiometers. Given the average typical brightness values of various ice types (see, for example, Ivanova et al., 2015), the variation of the two selected tangent values for SSMIS and AMSR2 frequencies amounts to less than 6%. Therefore, the use of another frequency set does not tangibly affect the shape of approximations equations (2), (3) and Eqs. (4), (5).

It should be noted that by using the relationship equation (6), the algorithm takes into account not all values of tangent 37–19 v for SWM, but only those that fall inside the area of the shaded triangle below the dashed line (Fig. 3). However, even for AMSR2, the pixel size at these frequencies is greater than 10 km. Patches of SWM can cover up to 50% of ice surface, their dimensions can reach hundreds of square meters. Thus, the area of an SWM patch is much less than that of a pixel. The value of tangent 37–19 v in a pixel is then determined by the additive sum of tangents for SWM and ice with their "weights". In this case the value of tangent 37–19 v falls in the shaded area below the dashed line (Fig. 3).

The use of tangents allows us to minimize the impact of atmospheric radiation, because only the slope of a straight line drawn through two values of brightness temperature is considered, but not the values themselves. Theoretical calculations show that total cross section of spherical ice particles (coated by water and uncoated ones) with diameter less than 1 mm is rather small, slightly increasing in the range from 20 to 100 GHz (Tikhonov et al., 2014). Therefore, in this range, the attenuation of radiation in snow clouds, snow, hail and snowstorms has weak frequency dependence. That is why snow precipitation affects brightness temperature of the upper atmosphere in a similar way within the entire frequency range considered. In this case, the tangents remain practically constant. This conclusion is confirmed in experimental and theoretical studies of microwave radiation attenuation in snow precipitation (Ishimaru, 1978; Matzler, 2006). Attenuation of microwave radiation in rain is large compared to attenuation in snow and has strong frequency dependence (Matzler, 2006). In the polar regions, about 75% of precipitation is snow, while rain occurs only in summer and mostly in ice-free areas. (Serreze and Barry, 2005; Palerme et al., 2014). Thus, the use of slope tangents as input parameters for the proposed algorithm significantly reduces the influence of atmospheric radiation and related weather phenomena.

3. Data

The required satellite data were taken from a collection of SSM/I and SSMIS data on Polar Regions, called POLE-RT-Fields, that was compiled on the basis of the GLOBAL-RT database developed at the Department of Earth Research from Space of the Space Research

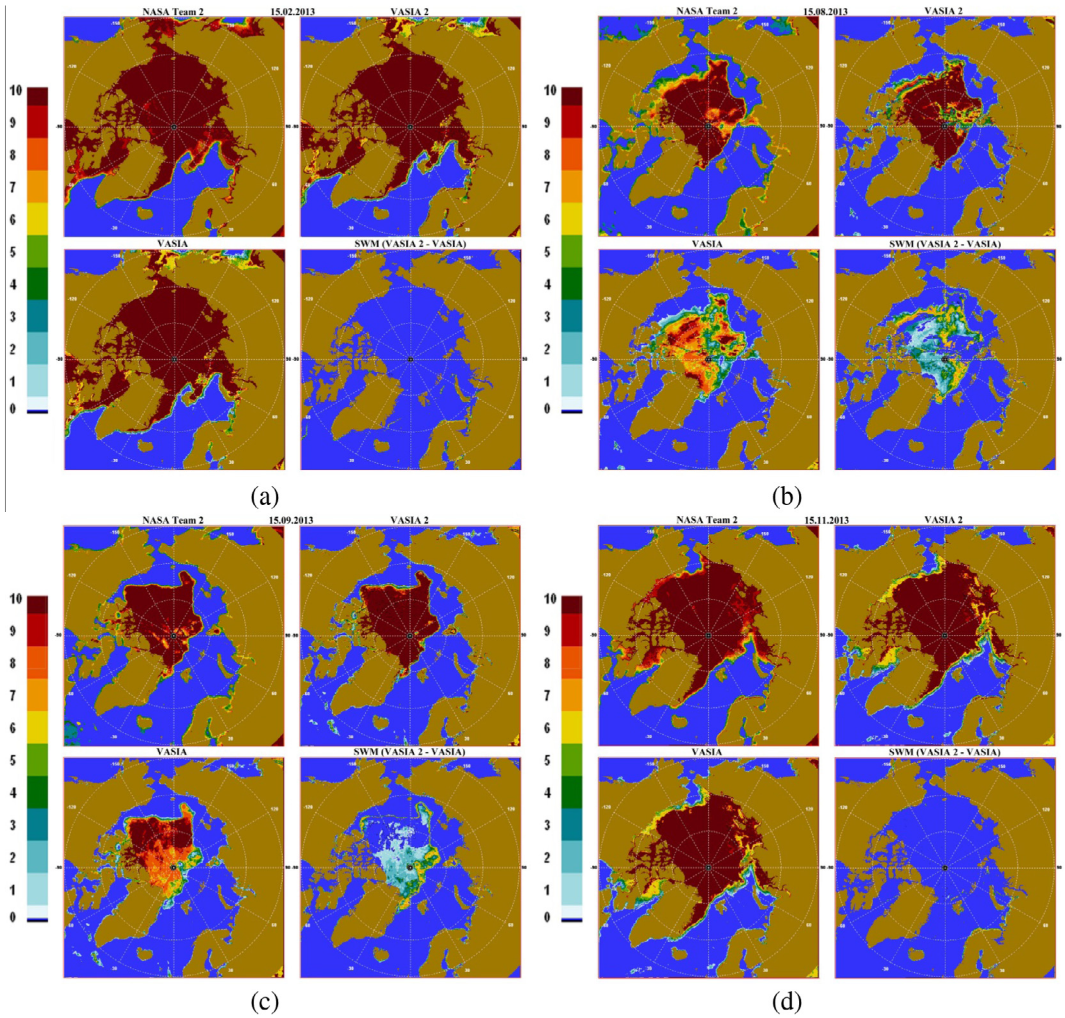

Fig. 4. Ice concentration (in 10ths) in the Arctic in 2013 calculated by algorithms NASA Team 2 (top row, left), VASIA2 (top row, right) and VASIA (bottom row, left), and the specific area of SWM (bottom row, right) on: (a) 15 February 2013, (b) 15 August 2013, (c) 15 September 2013, (d) 15 November 2013.

Institute of the Russian Academy of Sciences (Sharkov, 2003; Tikhonov et al., 2014). The source data for processing were brightness temperature data obtained by SSM/I and SSMIS multiband instruments of the DMS (Defense Meteorological Satellite) Program. These are free-access data supplied by The National Snow and Ice Data Center at http://sidads.colorado.edu/pub/datasets/. The data are represented in polar coordinate system separately for the north and south hemispheres. The resolution for the high frequency bands of 85 (91) GHz is 12.5 km, for the 19–37 GHz bands 25 km.

Ice concentration computing by NASA Team 2 algorithm was performed according to well-known detailed descriptions (see, for example, Markus and Cavalieri, 2009).

The validation of the proposed algorithm was performed using ice observations of the Arctic and Antarctic Research Institute (Alexeeva and Frolov, 2013). Summer observations were conducted during an expedition of RV "Akademik Frolov" in the Laptev, Kara and East-Siberian Seas. Winter data were obtained during an expedition of RV "Mikhail Somov" in the Kara Sea and Pechora Bay.

The observations involved visual identification of the main set of ice characteristics: age, total and partial concentration of each ice age type, form, thickness of level ice, thickness of snow cover, hummocking, disintegration, and compression of ice. Complete meteorological information was simultaneously gathered, including data on heat transfer through ice of different forms. As a rule, ice characteristics are estimated along the route of a ship, largely over the segments with easier navigation conditions: lower ice concentration, thinner ice, less hummocked ice, etc. So, there is a difference between observational data on ice along the ship route and in the area around it. To compare ship visual observation and satellite data, we used the total ice concentration obtained in the area surrounding the ship route.

Obviously, the ship and satellite data differ in spatial resolution. For comparison purpose, the ship route is divided

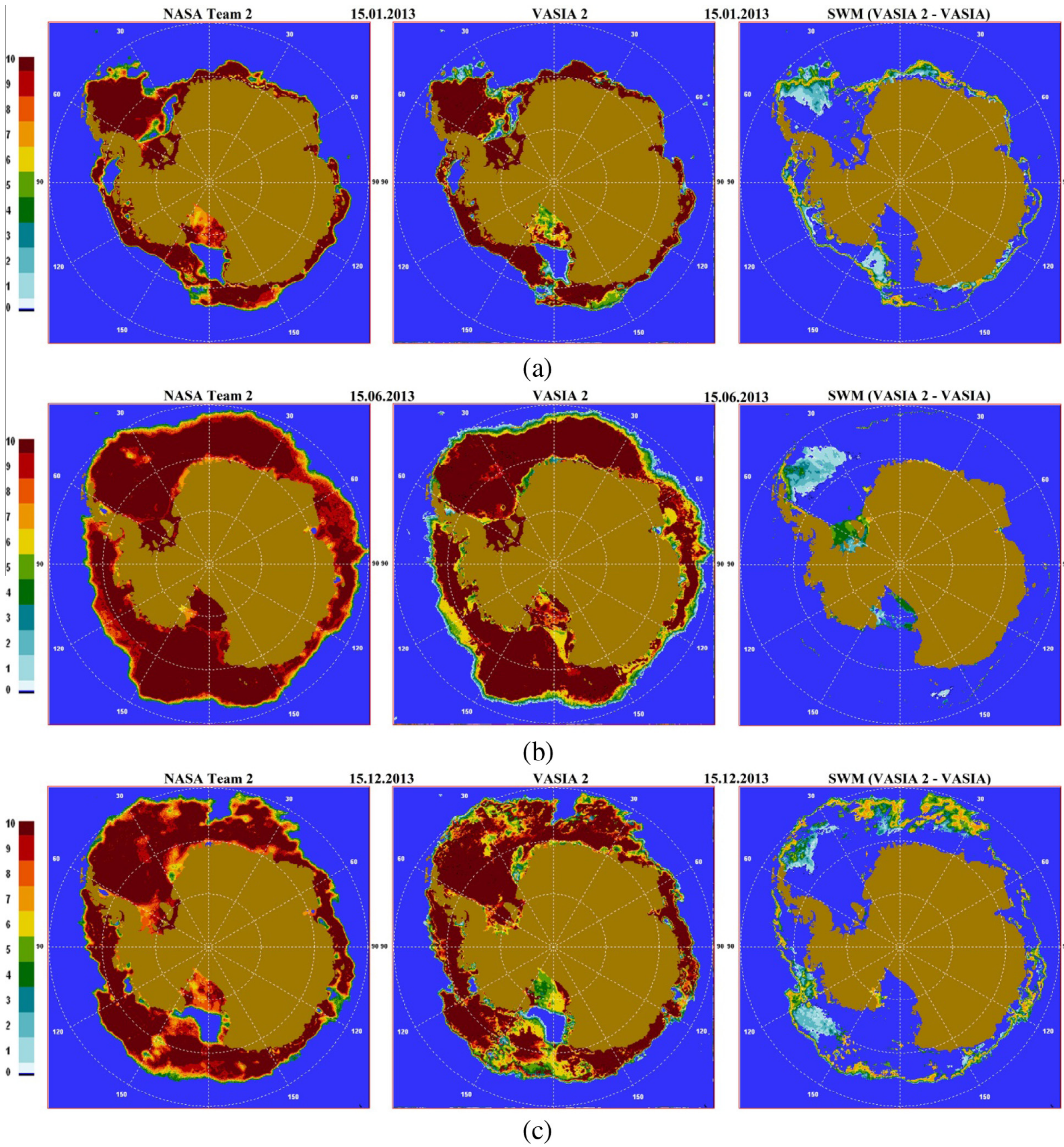

Fig. 5. Ice concentration (in 10ths) in the Southern Ocean in 2013 calculated by algorithms NASA Team2 (left) and VASIA2 (center), and the specific area of SWM (right) on (a) 15 January 2013, (b) 15 June 2013, (c) 15 December 2013.

into 1 km intervals. Total ice concentration is averaged over each interval. The resolution of SSM/I and SSMIS data is 25×25 km. One satellite image pixel therefore corresponds to several 1 km intervals. On the average, one pixel extends for 20–25 km of ship route. Under good visibility conditions, the observer determined total ice concentration over a circle area with a radius of 8–10 km. So, visual observation data covered from 51% to 64% of satellite data pixel area. Further, ice concentration average value by visual observations was calculated for each pixel. Observations made under poor visibility conditions (fog, heavy snow, nighttime) were discarded from the analysis.

4. Discussion

Ice concentrations reconstructed by algorithms VASIA and VASIA2 were compared with maps of ice concentration obtained by algorithm NASA Team 2 (NT2) (see Section 3).

Fig. 4 shows the map of the Arctic ice concentration obtained by algorithms NT2, VASIA2 and VASIA, and the area occupied by SWM (VASIA2–VASIA) for mid-February (a), August (b), September (c) and November (d) of 2013. Analysis of Fig. 4 shows that the overall pictures of ice fields produced by algorithms NT2

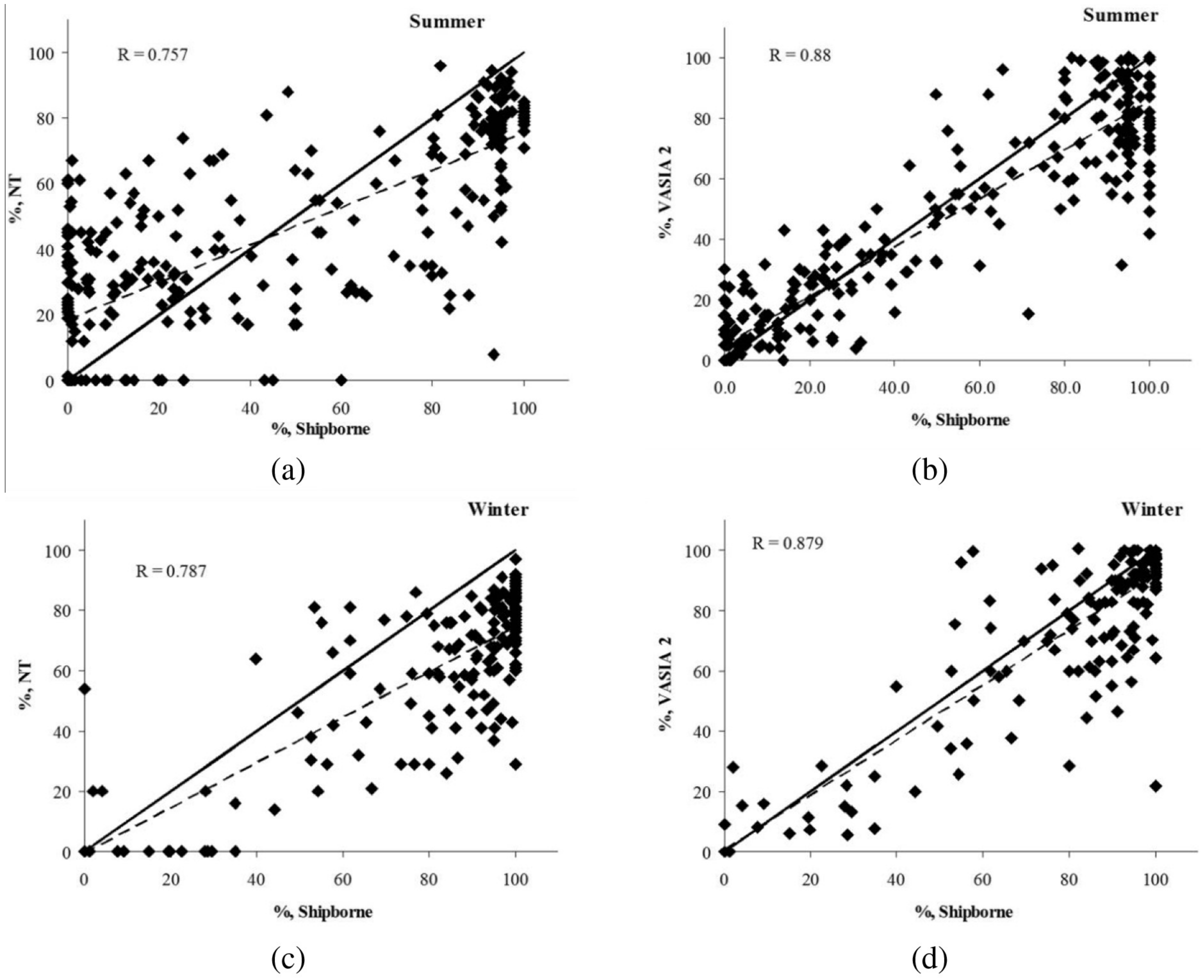

Fig. 6. Scatter plots of ice concentration versus visual observations and total ice concentration calculated by: (a) NT in summer; (b) VASIA2 in summer; (c) NT in winter; (d) VASIA2 in winter.

and VASIA2 are almost identical. The differences occur in the marginal ice zones where VASIA2 shows gradual transition from solid ice (100% ice concentration), through ice concentration variation, to open water. NT2 demonstrates a sharper transition: open water appears almost immediately after 80–100% ice concentration. VASIA underestimates ice concentration in warm months (Fig. 4(b) and (c)), which is explained by presence of SWM on the ice surface. In winter months (Fig. 4(a) and (d)), ice concentrations produced by all three algorithms are almost identical. There are no SWM in winter (Fig. 4(a) and (d)). The only exceptions are small stripes of sea ice along the east coast of Greenland and south of Franz Josef Land between Novaya Zemlya and Svalbard (Fig. 4(a)), as well as to the north of the Svalbard archipelago and at the east coast of Novaya Zemlya (Fig. 4(d)). These are the marginal ice zones (MIZ) where open water is in constant contact with the edge of ice. The water-soaked ice of the MIZ is well revealed by VASIA2. In summer months, SWM is found almost everywhere on the ice surface. Their number increases with distance from the Poles, as the climate becomes milder. At the periphery, SWM covers up to 60% of the ice surface (Fig. 4(b) and (c)).

VASIA2 algorithm shows good results in the Southern Ocean as well. Fig. 5 shows ice concentration around Antarctica, obtained by algorithms NT2 and VASIA2, and the area of SWM (VASIA2–VASIA), for mid-January (a), June (b) and December (c) in 2013. The results produced by algorithms NT2 and VASIA2 almost coincide. There are some differences along the ice edge only. Algorithm VASIA2 shows smooth transition of ice concentration across the MIZ, from solid ice to open water. In summer months, SWM occurs all over the ice edge (Fig. 5(a) and (c)). In the Antarctic, there are usually no melt ponds due to greater thickness of snow cover and colder and drier conditions (Thomas and Dieckmann, 2003). With summer heat flux from the ocean, the sea ice becomes thinner. Because of its mass, the snow cover can force the ice to move under the sea level. This leads to melting of the bottom snow layer at the ice–snow interface and formation of SWM (Eicken et al., 2004; Lewis et al., 2011). These areas are shown by VASIA2 in Fig. 5(a) and (c). In winter months, SWM are observed only in the region of

Antarctic Peninsular, where the climate is milder and warmer (Fig. 5(b)).

Comparison of total ice concentration derived from satellite data and ship observations is performed separately for summer and winter months of 2004 (Section 3). Fig. 6 presents scatter plots of total ice concentration by ship observations and algorithms NASA Team (NT) and VASIA2 for summer (Fig. 6(a) and (b)) and winter (Fig. 6(c) and (d)) months. The comparison shows high correlation coefficients for both periods, as well as high positive correlation.

For areas of scattered ice, both algorithms overestimate total ice concentration. For areas of close, very close and compact pack ice, the algorithms underestimate it. For low concentrations, the discrepancy by NT is bigger than that by VASIA2. The correlation of VASIA2 values is better both for the summer and winter periods. As is clear from Fig. 6, the points in VASIA2 correlation plots are distributed in a more chaotic manner, which results in compensation of the positive and negative errors when calculating the mean error.

5. Conclusions

A conceptually new algorithm VASIA2 of sea ice concentration retrieval from satellite microwave radiometry data is presented. The algorithm is based solely on a theoretical model and calculations. The analysis of the model of emission of the "sea surface – sea ice – snow cover – atmosphere" system developed by the authors (Tikhonov et al., 2014) has pointed out parameters essentially determined by ice concentration. These are tangents 85–19 v and 85–37 h, They are the basis of VASIA2. The algorithm does not use tie-points whose identification is the core task of most other algorithms currently employed. The design of VASIA2 practically precludes the effect of atmospheric variation on the calculation results. VASIA2 calculates not only sea ice concentration, but also areas occupied by snow–water mixture (SWM), i.e. water-soaked snow and melt ponds. This property opens a way for a more accurate analysis of climate change in Polar Regions.

Comparison of total concentration maps derived for the Arctic and Antarctic by NASA Team2 and VASIA2 algorithms has demonstrated their good agreement. This confirms validity of the emission model of the "sea surface – sea ice – snow cover – atmosphere" system (Tikhonov et al., 2014).

Comparison of VASIA2 results with ship observations in the Arctic in summer and winter months has yielded high correlation coefficients. However, in summer the algorithm overestimates the total ice concentration in regions with low concentration and underestimates it in regions with high concentration.

Further analysis and comparisons of VASIA2 performance with ship observations, high resolution radiometry, radar and infrared data are necessary to assess more accurately its drawbacks and advantages.

Acknowledgement

The authors would like to thank the research scientist Tatyana Bocharova (Department of Earth Research from Space, Space Research Institute Russian Academy of Sciences) for the great help with the translation of the manuscript into English.

This work was supported by the Russian Foundation for Basic Research, Grant RFBR No. 13-05-00272, Grant RFBR No. 13-05-41443, Grant RFBR No. 14-05-00039.

References

Agnew, T., Howell, S., 2003. The use of operational ice charts for evaluating passive microwave ice concentration data. Atmos.-Ocean. 41 (4), 317–331. http://dx.doi.org/10.3137/ao.410405.

Alexeeva, T.A., Frolov, S.V., 2013. Comparative analysis of satellite and shipborne data on ice cover in the Russian Arctic sea. Izvestia Atmos. Ocean. Phys., Исследования Земли из космоса 49 (9), 879–885. http://dx.doi.org/10.1134/S000143381309017X.

Andersen, S., 1998. Monthly Arctic Sea ice signatures for use in passive microwave algorithms. Danish Meteorological Institute. Technical report 98-18, 29 p. <http://saf.met.no/docs/tiepoints.pdf>.

Andersen, S., Tonboe, R., Kern, S., Schyberg, H., 2006. Improved retrieval of sea ice total concentration from spaceborne passive microwave observations using numerical weather prediction model fields: an intercomparison of nine algorithms. Remote Sens. Environ. 104 (4), 374–392. http://dx.doi.org/10.1016/j.rse.2006.05.013.

Andersen, S., Tonboe, R., Kaleschke, L., Heygster, G., Pedersen, L.T., 2007. Intercomparison of passive microwave sea ice concentration retrievals over the high-concentration Arctic sea ice. J. Geophys. Res. 112, C08004. http://dx.doi.org/10.1029/2006JC003543.

Boyarskii, D.A., Tikhonov, V.V., 2000. The influence of stratigraphy on microwave radiation from natural snow cover. J. Electromagn. Waves Appl. 14 (9), 1265–1285.

Boyarskii, D.A., Tikhonov, V.V., Kleeorin, N.I., Mirovskii, V.G., 1994. Inclusion of scattering losses in the models of the effective permittivity of dielectric mixtures and applications to wet snow. J. Electromagn. Waves Appl. 8 (11), 1395–1410.

Carsey, F.D. (Ed.), 1992. Microwave Remote Sensing of Sea Ice. American Geophysical Union, Washington, p. 462.

Cavalieri, D.J., Comiso, J.C., 2000. Algorithm theoretical basis document (ATBD) for the AMSR-E sea ice algorithm. Goddard Space Flight Center, Landover, Maryland USA, 79 p. <http://nsidc.org/data/amsre/pdfs/amsr_atbd_seaice.pdf>.

Cavalieri, D.J., Gloersen, P., Wilheit, T.T., 1986. Aircraft and satellite passive microwave observations of the Bering Seaice cover during MIZEX West. IEEE Trans. Geosci. Remote Sens. GE-24 (3), 368–377.

Cavalieri, D.J., Germain, K.M. St., Swift, C.T., 1995. Reduction of weather effects in the calculation of sea ice concentration with the DMSP SSM/I. J. Glaciol. 41, 455–464.

Cho, K., Nishiura, K., 2010. A study on cloud effect reduction for extracting sea ice area from passive microwave sensor data. Int. Arch. Photogrammetry Remote Sens. Spatial Inf. Sci. XXXVIII (8), 1042–1045.

Choudhury, B.J., Schmugge, T.J., Chang, A., Newton, R.W., 1979. Effect of surface roughness on the microwave emission from soils. J. Geophys. Res. 84 (C9), 5699–5706.

Comiso, J.C., 1995. SSM/I concentrations using the bootstrap algorithm. NASA Reference Publication 1380, 50 p.

Comiso, J.C., 2009. Polar Oceans from Space (Atmospheric and Oceanographic Sciences Library). Springer, New York, 507 p.

Comiso, J.C., Kwok, R., 1996. Surface and radiative characteristics of the summer Arctic sea cover from multisensor satellite observations. J. Geophys. Res. 101 (C12), 28397–28416.

Comiso, J.C., Grenfell, T.C., Bell, D.L., Lange, M.A., Ackley, S.F., 1989. Passive microwave in situ observations of winter Weddell sea ice. J. Geophys. Res. 94 (C8), 10891–10905.

Cuffey, K.M., Paterson, W.S.B., 2010. The Physics of Glaciers. Elsevier, 704 p.

Drinkwater, M.R., Crawford, J.P., Cavalieri, D.J., 1991. Multi-frequency, multi-polarization SAR and radiometer sea ice classification. In: Proceeding of International Geoscience and Remote Sensing Symposium (IGARSS'91), New York, USA, vol. I, pp. 107–111.

Eicken, H., Grenfell, N.C., Perovich, D.K., Richter-Menge, J.A., Frey, K., 2004. Hydraulic controls of summer Arctic pack ice albedo. J. Geophys. Res. 109 (C08007). http://dx.doi.org/10.1029/2003JC001989.

Fetterer, F., Untersteiner, N., 1998. Observations of melt ponds on Arctic sea ice. J. Geophys. Res.-Oceans 103 (C11), 24821–24835.

Fliickiger, K., Gmiinder, H., Matzler, Ch., 1994. Microwave signatures of sea ice from ARKTIS 93 experiment. EARSeL Adv. Remote Sens. 3 (2-XII), 71–80.

Gray, D.M., Male, D.H. (Eds.), 1981. Handbook of Snow: Principles, Processes, Management and Use. Pergamon Press, Toronto, p. 776.

Grenfell, T.C., 1986. Surface-based passive microwave observations of sea ice in the Bering and Greenland seas. IEEE Trans. Geosci. Remote Sens. GE-24 (3), 378–382.

Grenfell, T.C., 1992. Surface-based passive microwave studies of multi-year sea ice. J. Geophys. Res.: Oceans 97 (C3), 3485–3501.

Grenfell, T.C., Comiso, J.C., 1986. Multifrequency passive microwave observations of first-year sea ice grown in a tank. IEEE Trans. Geosci. Remote Sens. GE-24 (6), 826–831.

Grenfell, T.C., Perovich, D.K., 1984. Spectral albedos of sea ice and incident solar irradiance in the Southern Beaufort sea. J. Geophys. Res. 89 (C3), 3575–3580.

Hallikainen, M.T., Ulaby, F.T., Abdelrazik, M., 1986. Dielectric properties of snow in the 3 to 37 GHz range. IEEE Trans. Antennas Propagat. 34 (11), 1329–1339.

Han, H., Lee, H., 2006. Comparison of SSM/I sea ice concentration with kompsat-1 eoc images of the arctic and antarctic. In: IEEE International Geoscience and Remote Sensing Symposium, IGARSS 2006, Denver, CO, pp. 714–717. http://dx.doi.org/10.1109/IGARSS.2006.187.

Hewison, T.J., Selbach, N., Heygster, G., Taylor, J.P., McGrath, A.J., 2002. Airborne measurements of Arctic sea ice, glacier and snow emissivity at 24–183 GHz. In: Proceeding IEEE International Geoscience and Remote Sensing Symposium, IGARSS '02, vol. 5, pp. 2851–2855.

Ishimaru, A., 1978. Wave Propagation and Scattering in Random Media. Academic Press, New York, 572 p.

Istomina, L., Heygster, G., Huntemann, M., Schwarz, P., Birnbaum, G., Scharien, R., Polashenski, C., Perovich, D., Zege, E., Malinka, A., Prikhach, A., Katsev, I., 2011. The melt pond fraction and spectral sea ice albedo retrieval from MERIS data: validation and trends of sea ice albedo and melt pond fraction in the Arctic for years 2002–2011. The Cryosphere Discussions, vol. 8, pp. 5227–5292. http://dx.doi.org/10.5194/tcd-8-5227-2014.

Ivanova, N.O., Johannessen, M., Pedersen, L.T., Tonboe, R.T., 2014. Retrieval of arctic sea ice parameters by satellite passive microwave sensors: a comparison of eleven sea ice concentration algorithms. IEEE Trans. Geosci. Remote Sens. 52 (11), 7233–7246. http://dx.doi.org/10.1109/TGRS.2014.2310136.

Ivanova, N.O., Pedersen, L.T., Tonboe, R.T., Kern, S., Heygster, G., Lavergne, T., Sørensen, A., Saldo6, R., Dybkjær, G., Brucker, L., Shokr, M., 2015. Satellite passive microwave measurements of sea ice concentration: an optimal algorithm and challenges. In: The Cryosphere Discussions, vol. 9, pp. 1296–1313. http://dx.doi.org/10.5194/tcd-9-1269-2015.

Kaleschke, L., Lupkes, C., Vihma, T., Haarpaintner, J., Bochert, A., Hartmann, J., Heygster, G., 2001. SSM/I sea ice remote sensing for mesoscale ocean-atmosphere interaction analysis. Can. J. Remote Sens. 27 (5), 526–537.

Kern, S., 2004. A new method for medium-resolution sea ice analysis using weather-influence corrected special sensor microwave/imager 85 GHz data. Int. J. Remote Sens. 25, 1–28.

Knuth, M.A., Ackley, S.F., 2006. Summer and early-fall sea-ice concentration in the Ross Sea: comparison of in situ ASPeCt observations and satellite passive microwave estimates. Ann. Glaciol. 4 (1), 303–309. http://dx.doi.org/10.3189/172756406781811466.

Kotlyakov, V.V., 2000. Glaciology of Antarctica. Nauka, Moscow (Selected works in six books. Book 1. In Russian) 432 p.

Kuz'min, P.P., 1957. The Physical Properties of Snow Cover. Gidrometeoizdat, Leningrad (In Russian) 180 p.

Lewis, M.J., Tison, J.L., Weissling, B., Delille, B., Ackley, S.F., Brabant, F., Xie, H., 2011. Sea ice and snow cover characteristics during the winter-spring transition in the Bellingshausen Sea: an overview of SIMBA 2007. Deep Sea Res. Part II: Topical Stud. Oceanogr. 58 (9–10), 993–1276 (Antarctic Sea Ice Research during the International Polar Year 2007–2009, pp. 1019–1038).

Lovas, S.M., Rubinstein, I., Ulstad, C., 1994. Weather influence on passive microwave brightness temperatures. Polar Res. 13 (1), 67–81.

Markus, T., Cavalieri, D.J., 2009. The AMSR-E NT2 Sea ice concentration algorithm·its basis and implementation. J. Remote Sens. Soc. Jpn. 29 (1), 216–225.

Massom, R., Lubin, D., 2006. Polar remote sensing. Ice Sheets, vol. II. Springer – Praxis Publishing, Chichester, 426 p.

Matzler, C. (Ed.), 2000. Radiative transfer models for microwave radiometry. COST 712: Final Report of Project 1. Bern, Switzerland, p. 176.

Matzler, C. (Ed.), 2006. Thermal Microwave Radiation: Applications for Remote Sensing. The Institution of Electrical Engineers, London, p. 584.

Matzler, C., Huppi, R., 1989. Review of signature studies for microwave remote sensing of snowpacks. Adv. Space Res. 9 (1), (1)253–(1)265.

Meier, W.N., 2005. Comparison of passive microwave ice concentration algorithm retrievals with AVHRR imagery in Arctic Peripheral Seas. IEEE Trans. Geosci. Remote Sens. 43 (6), 1324–1337.

Meier, W.N., Van Woert, M.L., Bertoial, C., 2001. Evaluation of operational SSM/I ice-concentration algorithms. Ann. Glaciol. 33, 102–108.

Morassutti, M.F., Ledrew, E.F., 1996. Albedo and depth of melt ponds on sea-ice. International Journal of Climatology 16, 817–838.

Onstott, R.G., Grenfell, T.C., Matzler, C., Luther, C.A., Svendsen, E.A., 1987. Evolution of microwave sea ice signatures during early summer and midsummer in the marginal ice zone. J. Geophys. Res. 92 (C7), 6825–6835.

Palerme, C., Kay, J.E., Genthon, C., L'Ecuyer, T., Wood, N.B., Claud, C., 2014. How much snow falls on the Antarctic ice sheet? Cryosphere 8 (4), 1577–1587.

Pedersen, L.T., 1994. Merging microwave radiometer data and meteorological data for improved sea ice concentrations. EARSeL Adv. Remote Sens. 3 (2-XII), 81–89.

Perovich, D.K., Grenfell, T.G., Richter-Menge, J.A., Light, B., Tucker III, W.B., Eicken, H., 2003. Thin and thinner: sea ice mass balance measurements during SHEBA. J. Geophys. Res. 108 (C03). http://dx.doi.org/10.1029/2001JC001079.

Polashenski, C., Perovich, D., Courville, Z., 2012. The mechanisms of sea ice melt pond formation and evolution. J. Geophys. Res. 117 (C01001). http://dx.doi.org/10.1029/2011JC007231.

Polder, D., van Santen, J.H., 1946. The effective permeability of mixtures of solids. Physica 12 (5), 257–271.

Powell, D.C., Markus, T., Cavalieri, D.J., Gasiewski, A.J., Klein, M., Maslanik, J.A., Stroeve, J.C., Sturm, Mathew, 2006. Microwave signatures of snow on sea ice: modeling. IEEE Trans. Geosci. Remote Sens. 44 (11), 3091–3102.

Przybylak, R., 2003. The Climate of the Arctic. Kluwer Academic Publishers, Dordrecht, 271 p.

Rees, W.G., 2006. Remote Sensing of Snow and Ice. Taylor & Francis Group, New York, 285 p.

Rösel, A., Kaleschke, L., 2012. Exceptional melt pond occurrence in the years 2007 and 2011 on the Arctic sea ice revealed from MODIS satellite data. J. Geophys. Res. 117 (C05018). http://dx.doi.org/10.1029/2011JC007869.

Rösel, A., Kaleschke, L., Birnbaum, G., 2012. Melt ponds on Arctic sea ice determined from MODIS satellite data using an artificial neural network. Cryosphere (6), 431–446. http://dx.doi.org/10.5194/tc-6-431-2012.

Serreze, M., Barry, R., 2005. The Arctic Climate System. University Press, Cambridge, 385 p.

Sharkov, E.A., 2003. Passive Microwave Remote Sensing of the Earth: Physical Foundations. Springer/PRAXIS, Berlin, Heidelberg, London, New York etc, 613 p.

Shokr, M., Lambe, A., Agnew, T., 2008. A new algorithm (ECICE) to estimate ice concentration from remote sensing observations: an application to 85 GHz passive microwave data. IEEE Trans. Geosci. Remote Sens. 46 (12), 4104–4121.

Sihvola, A.H., Kong, J.A., 1988. Effective permittivity of dielectric mixtures. IEEE Trans. Geosci. Remote Sens. 26 (4), 420–429.

Spreen, G., Kaleschke, L., Heygster, G., 2008. Sea ice remote sensing using AMSR-E 89-GHz channels. J. Geophys. Res. 113 (C02S03). http://dx.doi.org/10.1029/2005JC003384.

Svendsen, E., Kloster, K., Farrelly, B., Johannessen, O.M., Johannessen, J.A., 1983. Norwegian remote sensing experiment: evaluation of the nimbus 7 scanning multichannel microwave radiometer for sea ice research. J. Geophys. Res. 88 (C5), 2781–2791.

Swift, C.T., Germain, K.St., Jezek, K.C., Gogineni, S.P., Gow, A.J., Perovich, D.K., Grenfell, T.C., Onstott, R.G., 1992. Laboratory investigations of the electromagnetic properties of artificial sea ice. In: Carsey, F.D. (Ed.), Microwave Remote Ssensing of Sea Ice. American Geophysical Union, Washington, pp. 61–84 (chapter 9).

Teleti, P.R., Luis, A.J., 2013. Sea ice observations in polar regions: evolution of technologies in remote sensing. Int. J. Geosci. 4 (7), 1031–1050. http://dx.doi.org/10.4236/ijg.2013.47097.

Thomas, D.N., Dieckmann, G.S. (Eds.), 2003. Sea Ice. Blackwell Publishing.

Tikhonov, V.V., Boyarskii, D.A., Repina, I.A., Raev, M.D., Sharkov, E.A., Alexeeva, T.A., 2013. Snow cover effect on brightness temperature of arctic ice fields based on ssm/i data. In: Progress In Electromagnetics Research Symposium (PIERS) Proceedings, Stockholm, Sweden, pp. 514–518.

Tikhonov, V.V., Boyarskii, D.A., Sharkov, E.A., Raev, M.D., Repina, I.A., Ivanov, V.V., Alexeeva, T.A., Komarova, N.Yu, 2014. Microwave model of radiation from the multilayer “ocean-atmosphere” system for remote sensing studies of the polar regions. Progr. Electromagn. Res. B 59, 123–133.

Tschudi, M.A., Maslanik, J.A., Perovich, D.K., 2008. Derivation of melt pond coverage on Arctic sea ice using MODIS observations. Remote Sensing of Environment 112, 2605–2614. http://dx.doi.org/10.1016/j.rse.2007.12.009.

Tucker III, W.B., Grenfell, T.C., Onstott, R.G., Perovich, D.K., Gow, A.J., Shuchman, R.A., Sutherland, L.L., 1991. Microwave and physical properties of sea ice in the winter marginal ice zone. J. Geophys. Res. 96 (C3), 4573–4587.

Tucker III, W.B., Gow, A.J., Meese, D.A., Bosworth, H.W., 1999. Physical characteristics of summer sea ice across the Arctic Ocean. J. Geophys. Res. 104 (C1), 1489–1504.

Turner, John, Bindschadler, Robert, Convey, Pete, di Prisco, Guido, Fahrbach, Eberhard, Gutt, Julian, Hodgson, Dominic, Mayewski, Paul, Summerhayes, Colin (Eds.), 2009. Antarctic Climate Change and the Environment. Scientific Committee on Antarctic Research Scott Polar Research Institute. Cambridge, p. 526.

Voss, S., Heygster, G., Ezraty, R., 2003. Improving sea ice type discrimination by the simultaneous use of SSM/I and scatterometer data. Polar Res. 22 (1), 35–42.